Supporting Information

Anderson-like Alkoxo-polyoxovanadate Clusters Serving as Unprecedented Second Building Units to Construct Metal-organic Polyhedra

Yu-Teng Zhang, Xin-Long Wang,* Shuang-Bao Li, Ya-Ru Gong, Bai-Qiao Song, Kui-Zhan Shao, and Zhong-Min Su*

Institute of Functional Material Chemistry, Local United Engineering Lab for Power Battery, Northeast Normal University, Changchun, 130024 Jilin, People's Republic of China.

*Corresponding author. E-mail address: zmsu@nenu.edu.cn.

Contents

1. Materials and Methods

2. Synthesis and Characterization of VMOP-11~15

3. Single-crystal X-ray Crystallography

Table S1. Structural comparison of some typical vanadium-based metal-organic materials synthesized via different solvent systems.

Table S2−S6. Crystallographic data for **VMOP-11~15**.

Table S7. BVS results for the vanadium ions in **VMOP-11~15**.

Figure S1−S2. Packing arrangements of **VMOP-11** and **VMOP-14**.

Figure S3−S7. The experimental and simulated powder X-Ray diffraction patterns for **VMOP-11~15**.

Figure S8−S10. XPS spectra of **VMOP-11**, **VMOP-14** and **VMOP-15**.

Figure S11−S15. TGA curves of **VMOP-11~15**.

Figure S16−S20. IR spectra of **VMOP-11~15**.

Figure S21−S22. Temperature dependence of the inverse magnetic susceptibility χ_M^{-1} for **VMOP-14** and **VMOP-15** between 2 and 300 K.

1. Materials and Methods

All the reagents were obtained from commercial sources and used without further purification. Powder X-ray diffraction (PXRD) measurement was recorded ranging from 5 to 40º at room temperature on a Siemens D5005 diffractometer with Cu-*Kα* (λ = 1.5418 Å). The C, H, and N elemental analyses were conducted on a Perkin-Elmer 2400CHN elemental analyzer. Thermogravimetric analysis (TGA) of the samples was performed using a Perkin-Elmer TG-7 analyzer heated from room temperature to 800 ºC under nitrogen at the heating rate of 10 °C·min^{-1}. The C, H, and N elemental analyses were conducted on a Perkin-Elmer 2400CHN elemental analyzer. IR spectrum was performed in the range 4000–400 cm^{-1} using KBr pellets on an Alpha Centaurt FT/IR spectrophotometer. X-ray photoelectron spectroscopy analyses were performed on a VG ESCALABMKII spectrometer with an Al-Kα (1486.6 eV) achromatic X-ray source. The vacuum inside the analysis chamber was maintained at 6.2×10^{-6} Pa during the analysis.

2. Synthesis and Characterization

(1) Synthesis of **VMOP-11**:

$VOSO_4 \cdot xH_2O$ (0.08 g) and 1,4-benzenedicarboxylate (0.02 g) in 2 ml DEF (N,N-Diethylformamide) and 1ml CH_3OH (methanol) were placed in a Parr Teflon-lined stainless steel vessel heated to 130 °C and held at this temperature for 2 days. After slow cooling to room temperature, yellowish-brown crystals were obtained (washed with DEF) with a yield of 70 % based on H_2BDC. Elemental analysis (%) cacld: C, 30.96; H, 5.16; N, 2.87. Found: C, 30.82; H, 5.35; N, 2.58. IR (KBr, cm^{-1}): 3430 (br), 2931 (w), 2815 (w), 2499 (w), 1564(w), 1589 (vs), 1402 (vs), 1201 (w), 1080 (m), 954 (s), 744 (w), 649 (w), 570 (w).

(2) Synthesis of **VMOP-12**:

The synthetic procedure is similar to that of **VMOP-11** except that H_2BDC was replaced by 2-amino-1,4-benzenedicarboxylate. $VOSO_4 \cdot xH_2O$ (0.08 g) and $H_2BDC\text{-}NH_2$ (0.03 g) in 2 ml DEF and 1ml CH_3OH were placed in a Parr Teflon-lined stainless steel vessel heated to 130 °C and held at this temperature for 2 days. After slow cooling to room temperature, yellowish-brown crystals were obtained (washed with DEF) with a yield of 65 % based on $H_2BDC\text{-}NH_2$. Elemental

analysis (%) cacld: C, 30.10; H, 5.12; N, 4.41. Found: C, 29.92; H, 4.85; N, 4.58. IR (KBr, cm−1): 3484 (w), 3372 (w), 2931 (w), 2817 (w), 2497 (w), 1569 (s), 1440 (w), 1388 (w), 1205 (w), 1074 (s), 952 (s), 765 (w), 649 (w), 574 (w).

(3) Synthesis of **VMOP-13**:

The synthetic procedure is similar to that of **VMOP-11** except that H_2BDC was replaced by 2-bromo-1,4-benzenedicarboxylate (H_2BDC-Br). $VOSO_4 \cdot xH_2O$ (0.08 g) and H_2BDC-Br (0.035 g) in 2 ml DEF and 1ml CH_3OH were placed in a Parr Teflon-lined stainless steel vessel heated to 130 °C and held at this temperature for 2 days. After slow cooling to room temperature, yellowish-brown crystals were obtained (washed with DEF) with a yield of 42 % based on H_2BDC-Br. Elemental analysis (%) cacld: C, 27.63; H, 4.46; N, 2.40. Found: C, 27.86; H, 4.25; N, 2.58. IR (KBr, cm^{-1}): 3444 (br), 2929 (w), 2817 (w), 2499 (w), 1596 (s), 1398 (s), 1203 (w), 1079 (s), 950 (s), 763 (w), 647 (w), 576 (w), 539 (w).

(4) Synthesis of **VMOP-14**:

The synthetic procedure is similar to that of **VMOP-11** except that H_2BDC was replaced by tricarboxylate 1,3,5-benzentricarboxylate (H_3BTC). $VOSO_4 \cdot xH_2O$ (0.08 g) and H_3BTC (0.015 g) in 2 ml DEF and 1ml CH_3OH were placed in a Parr Teflon-lined stainless steel vessel heated to 130 °C and held at this temperature for 2 days. After slow cooling to room temperature, green crystals were obtained (washed with DEF) with a yield of 35 % based on H_3BTC. Elemental analysis (%) cacld: C, 27.93; H, 4.87; N, 2.60. Found: C, 27.76; H, 4.75; N, 2.76. IR (KBr, cm^{-1}): 3432 (br), 2931 (w), 2817 (w), 2497 (w), 1619 (s), 1571 (s), 1442 (s), 1384 (s), 1205 (w), 1076 (s), 950 (vs), 723 (s), 649 (w), 578 (w), 539 (w).

(5) Synthesis of **VMOP-15**:

The synthetic procedure is similar to that of **VMOP-11** except that H_2BDC was replaced by tricarboxylate 1, 3, 5-tris(4-carboxyphenyl)-benzene (H_3BTB). $VOSO_4 \cdot xH_2O$ (0.08 g) and H_3BTB (0.03 g) in 2 ml DEF and 1ml CH_3OH were placed in a Parr Teflon-lined stainless steel vessel heated to 130 °C and held at this temperature for 2 days. After slow cooling to room temperature, green crystals were obtained (washed with DEF) with a yield of 28 % based on H_3BTB. Elemental analysis (%) cacld: C, 39.39; H, 5.05; N, 2.38. Found: C, 39.16; H, 4.83; N, 2.47. IR (KBr, cm^{-1}): 3436 (br), 2929 (w), 2817 (w), 2495 (w), 1658 (w), 1591 (s), 1419 (vs), 1201 (w), 1076 (s), 954 (s), 775 (s), 647 (w), 574 (w), 539 (w).

3. Single-crystal X-ray Crystallography

The crystallographic data for **VMOP-11~15** are given in Table S2–S6. Intensity data were collected at 293 K on a Bruker APEX-II CCD diffractometer with graphite-monochromated Mo Kα radiation (λ = 0.71069 Å). Absorption corrections were applied using a multi scan technique. The structures were solved by direct methods with SHELXS-2014 and refined by full-matrix least squares techniques by the SHELXL-2014 program. The counter cations or disorder solvents cannot be exactly assigned from the weak reflections. Thus, the *SQUEEZE* program in *PLATON* was used to calculate and estimate the possible numbers of the cations and solvents in the accessible void of this crystal structure. During the refinement, most of the non-H atoms were refined ansiotropically. Additionally, in the final refinement, some restraints were used including DFIX, OMIT, SIMU and DELU. CCDC 1479717–1479721 contain the supplementary crystallographic data for this paper.

Table S1. Structural comparison of some typical vanadium-based metal-organic materials synthesized *via* different solvent systems.

	Solvent system [a]	Vanadium SBU	Structure	Ref
Vanadium-based metal organic materials synthesized by single solvent				
MIL-68	DMF	mononuclear	three-dimensional MOF	**1**
MIL-47	H_2O	mononuclear	three-dimensional MOF	**2**
MIL-59~61	H_2O	mononuclear	three-dimensional MOF	**3-4**
COMOC-2	DMF	mononuclear	three-dimensional MOF	**5**
V-MIL-101	DMF	trinuclear	three-dimensional MOF	**6**
Vanadium-based metal organic materials synthesized by mixed solvent				
VMOP-11	DEF+CH_3OH	$\{V_6S\}$	POV-based tetrahedral cage	**This wok**
Hyball-3	DMA+H_2O	$\{V_4Cl\}$	POV-based octahedral cage	**7**
Hyball-4	DBF+ H_2O	$\{V_5Cl\}$	POV-based octahedral cage	**7**
Hydoughnut-1	DEF +H_2O	$\{V_4Cl\}$	POV-based hydoughnut	**8**
Hydoughnut-2	DMF+H_2O	$\{V_4Cl\}$	POV-based hydoughnut	**8**
VMOP-1	DMF+CH_3CH_2OH	$\{V_5Cl\}$	POV-based octahedral cage	**9**

[a]DMF = N,N-dimethylformamide; DEF = N,N-diethylformamide; DMA = N,N-dimethylacetamide; DBF = N,N-dibutylformamide.

Table S2. Crystallographic data for **VMOP-11**

Empirical formula	$C_{126}H_{250}N_{10}O_{102}S_4V_{24}$
Formula weight	4888.15
Crystal system	Cubic

Space group	*I-43m*
Temperature	293(2) K
Wavelength	0.71069 Å
Unit-cell dimensions	a = b = c =21.927(5) Å α = β =γ = 90 °
Volume	10542(4) $Å^3$
Z	2
Density (calculated)	1.540 g/cm^3
Absorption coefficient	1.139 mm^{-1}
F(000)	5016
Limiting indices	-23<=h<=26, -26<=k<=26, -26<=l<=26
Theta range for data collection	1.31-25.00°
Reflections collected	30838
Independent reflections	1747 [R(int) = 0.0916]
Completeness to theta = 25.00°	100 %
Refinement method	Full-matrix least-squares on F^2
Data / restraints / parameters	1747 / 1 / 98
Goodness-of-fit on F^2	1.055
Final R indices [I > 2sigma(I)]	R1 = 0.0385, wR2 = 0.0860
R indices (all data)	R1 = 0.0477, wR2 = 0.0891
Largest diff. peak and hole	0.263 and -0.231 eA^{-3}

Table S3. Crystallographic data for **VMOP-12**

Empirical formula	$C_{123.5}H_{250.5}N_{15.5}O_{101.5}S_4V_{24}$
Formula weight	4927.68
Crystal system	Cubic
Space group	*I-43m*
Temperature	293(2) K
Wavelength	0.71069 Å
Unit-cell dimensions	a = b = c =21.841(5) Å α = β =γ = 90 °
Volume	10419(4) $Å^3$
Z	2
Density (calculated)	1.571 g/cm^3
Absorption coefficient	1.154 mm^{-1}
F(000)	5056
Limiting indices	-25<=h<=24, -25<=k<=25, -25<=l<=21
Theta range for data collection	1.32-24.99°
Reflections collected	30504
Independent reflections	1725 [R(int) = 0.0565]

Completeness to theta = 24.99°	100 %
Refinement method	Full-matrix least-squares on F^2
Data / restraints / parameters	1725 / 6 / 102
Goodness-of-fit on F^2	1.079
Final R indices [I > 2sigma(I)]	R1 = 0.0415, wR2 = 0.1011
R indices (all data)	R1 = 0.0480, wR2 = 0.1044
Largest diff. peak and hole	0.323 and -0.203 eA^{-3}

Table S4. Crystallographic data for **VMOP-13**

Empirical formula	$C_{121}H_{152}Br_6O_{101}S_4V_{24}$
Formula weight	5052.68
Crystal system	Cubic
Space group	*I-43m*
Temperature	293(2) K
Wavelength	0.71069 Å
Unit-cell dimensions	a = b = c =22.108(5) Å α = β =γ = 90 °
Volume	10806(4) $Å^3$
Z	2
Density (calculated)	1.553 g/cm^3
Absorption coefficient	2.215 mm^{-1}
F(000)	5024
Limiting indices	-26<=h<=25, -25<=k<=26, -26<=l<=23
Theta range for data collection	1.30-24.97°
Reflections collected	31352
Independent reflections	1787 [R(int) = 0.1085
Completeness to theta = 24.97°	100 %
Refinement method	Full-matrix least-squares on F^2
Data / restraints / parameters	1787 / 6 / 113
Goodness-of-fit on F^2	1.042
Final R indices [I > 2sigma(I)]	R1 = 0.0427, wR2 = 0.0990
R indices (all data)	R1 = 0.0543, wR2 = 0.1033
Largest diff. peak and hole	0.498 and -0.659 eA^{-3}

Table S5. Crystallographic data for **VMOP-14**

Empirical formula	$C_{106.50}H_{221.5}N_{8.5}O_{100.5}S_4V_{24}$
Formula weight	4580.21
Crystal system	Tetragonal
Space group	*I-4*
Temperature	293(2) K
Wavelength	0.71069 Å

Unit-cell dimensions	a = b = 21.848(5) Å c =19.081(5) Å α = β =γ = 90 °
Volume	9108(4) $Å^3$
Z	2
Density (calculated)	1.670 g/cm^3
Absorption coefficient	1.311 mm^{-1}
F(000)	4680
Limiting indices	-24<=h<=25, -25<=k<=24, -18<=l<=22
Theta range for data collection	1.32-25.00°
Reflections collected	26422
Independent reflections	8051 [R(int) = 0.0600]
Completeness to theta = 24.99°	100 %
Refinement method	Full-matrix least-squares on F^2
Data / restraints / parameters	8051 / 10 / 451
Goodness-of-fit on F^2	0.921
Final R indices [I > 2sigma(I)]	R1 = 0.0442, wR2 = 0.0951
R indices (all data)	R1 = 0.0668, wR2 = 0.1021
Largest diff. peak and hole	0.318 and -0.343 eA^{-3}

Table S6. Crystallographic data for **VMOP-15**

Empirical formula	$C_{183.5}H_{280..5}N_{9.5}O_{101.5}S_4V_{24}$
Formula weight	5594.46
Crystal system	Tetragonal
Space group	*I-4*
Temperature	293(2) K
Wavelength	0.71069 Å
Unit-cell dimensions	a = b = 28.983(5) Å c =25.744(5) Å α = β =γ = 90 °
Volume	21625(7) $Å^3$
Z	2
Density (calculated)	0.859 g/cm^3
Absorption coefficient	0.561 mm^{-1}
F(000)	5752
Limiting indices	-33<=h<=31, -33<=k<=33, -28<=l<=30
Theta range for data collection	0.99-24.50°
Reflections collected	60011
Independent reflections	17997 [R(int) = 0.0886]
Completeness to theta = 24.99°	100 %
Refinement method	Full-matrix least-squares on F^2
Data / restraints / parameters	17997 / 6 / 607

Goodness-of-fit on F^2	0.714
Final R indices [I > 2sigma(I)]	R1 = 0.0399, wR2 = 0.0683
R indices (all data)	R1 = 0.1056, wR2 = 0.0777
Largest diff. peak and hole	0.135 and -0.174 eA^{-3}

Table S7. BVS results for the vanadium ions in **VMOP-11~15**.

Atom	**BVS calc. for V(IV)**	**BVS calc. for V(V)**
*BVS results in **VMOP-11***		
V1	**4.23**	4.45
*BVS results in **VMOP-12***		
V1	**4.24**	4.47
*BVS results in **VMOP-13***		
V1	**4.19**	4.41
*BVS results in **VMOP-14***		
V1	**4.18**	4.40
V2	**4.23**	4.45
V3	**4.22**	4.44
V4	**4.21**	4.43
V5	**4.19**	4.41
V6	**4.23**	4.45
*BVS results in **VMOP-15***		
V1	**4.24**	4.46
V2	**4.08**	4.30
V3	**4.18**	4.40
V4	**4.30**	4.52
V5	**4.13**	4.34
V6	**4.17**	4.38

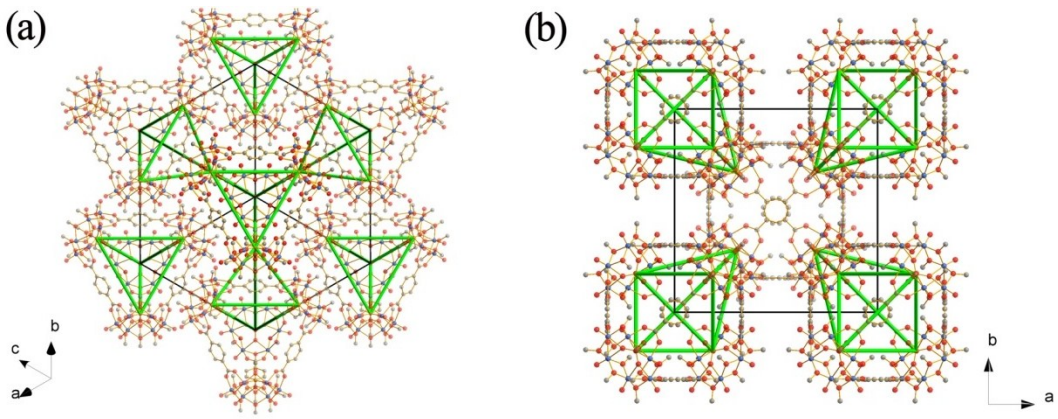

Figure S1. Packing arrangements of **VMOP-11** with views in different directions (the unit cell is outlined in black). Color code: V, light blue; S, orange; O, red; C, gray. For clarity, hydrogen atoms of methoxo CH_3O^- ligand are omitted. The vertexes of the green tetrahedra are drawn using the crystallographic positions of the central sulphur atoms of $\{V_6O_6(OCH_3)_9(\mu_6\text{-}SO_4)\}$ clusters.

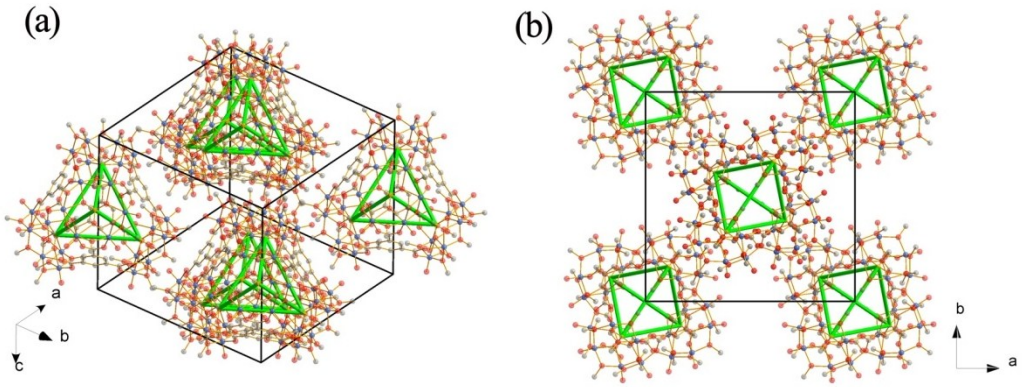

Figure S2. Packing arrangements of **VMOP-14** with views in different directions (the unit cell is outlined in black). Color code: V, light blue; S, orange; O, red; C, gray. For clarity, hydrogen atoms of methoxo CH_3O^- ligand are omitted. The vertexes of the green tetrahedra are drawn using the crystallographic positions of the central sulphur atoms of $\{V_6O_6(OCH_3)_9(\mu_6\text{-}SO_4)\}$ clusters.

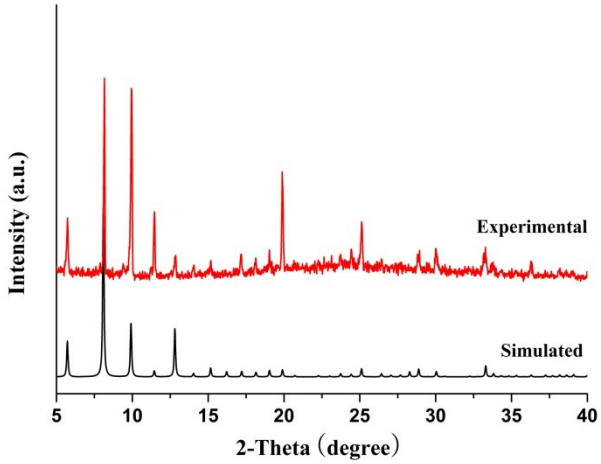

Figure S3. Experimental and simulated powder X-Ray diffraction patterns for **VMOP-11**.

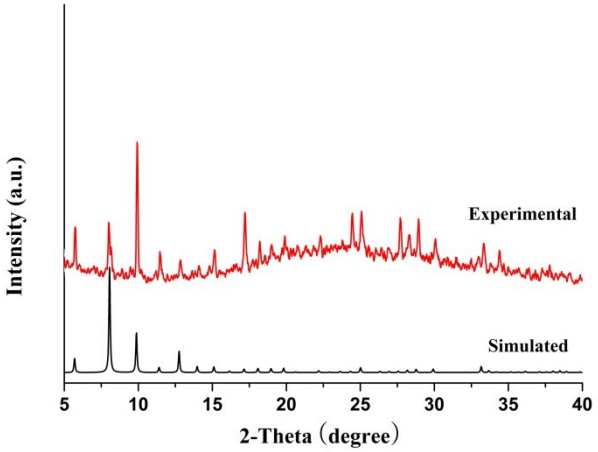

Figure S4. Experimental and simulated powder X-Ray diffraction patterns for **VMOP-12**.

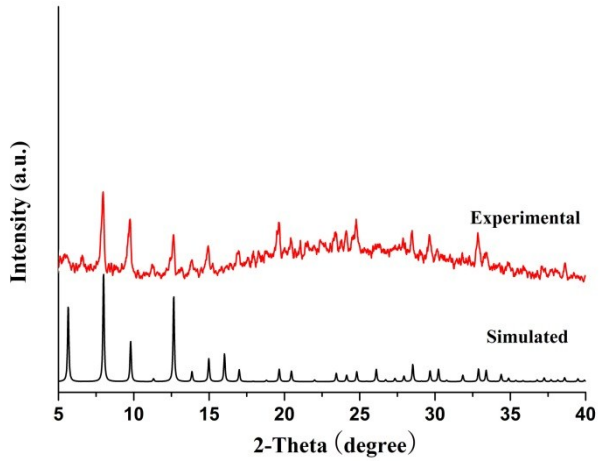

Figure S5. Experimental and simulated powder X-Ray diffraction patterns for **VMOP-13**.

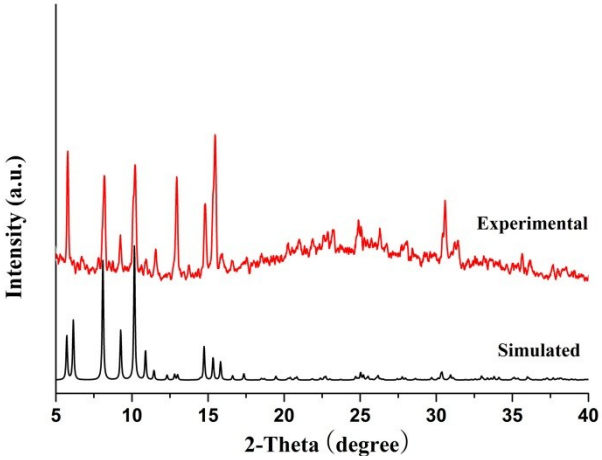

Figure S6. Experimental and simulated powder X-Ray diffraction patterns for **VMOP-14**.

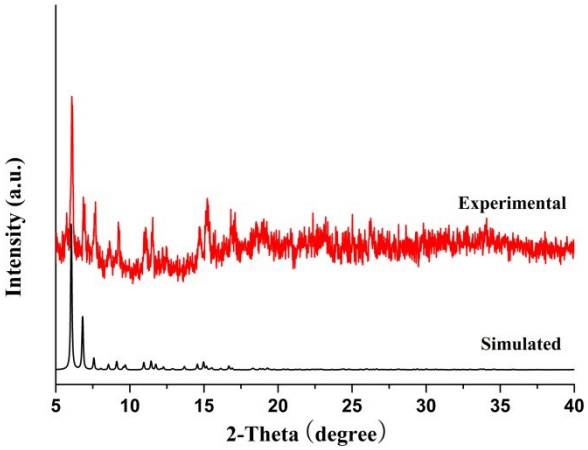

Figure S7. Experimental and simulated powder X-Ray diffraction patterns for **VMOP-15**.

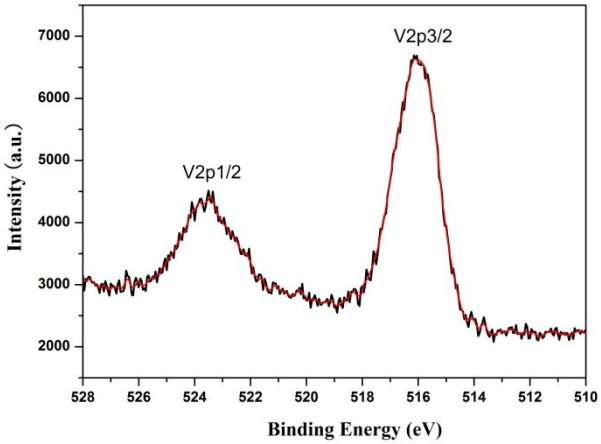

Figure S8. The XPS spectrum of **VMOP-11** gives one peak at 516.2 eV, which can be ascribed to V^{4+} $2p_{3/2}$.[10]

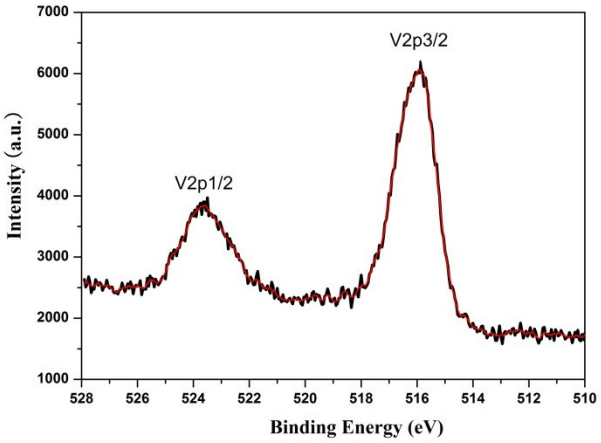

Figure S9. The XPS spectrum of **VMOP-14** gives one peak at 516.0 eV, which can be ascribed to V^{4+} $2p_{3/2}$.[10]

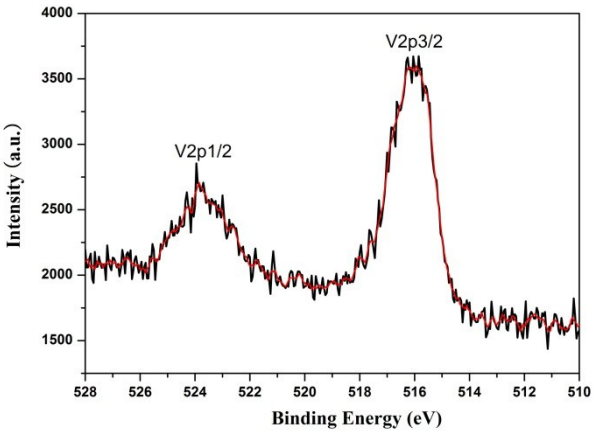

Figure S10. The XPS spectrum of **VMOP-15** gives one peak at 516.1 eV, which can be ascribed to V^{4+} $2p_{3/2}$.[10]

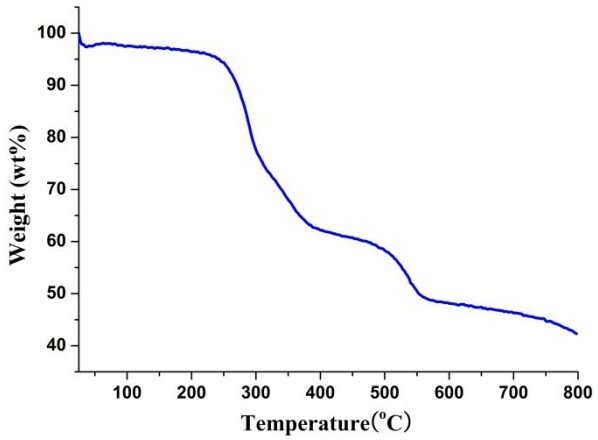

Figure S11. TGA curve of **VMOP-11.**

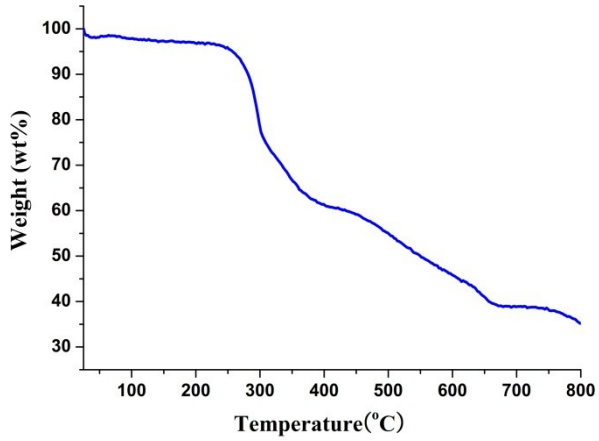

Figure S12. TGA curve of **VMOP-12.**

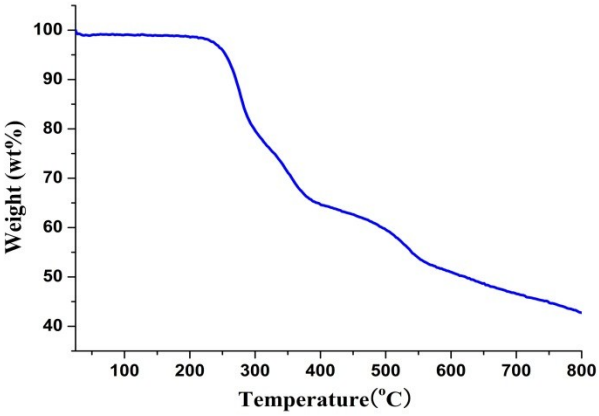

Figure S13. TGA curve of **VMOP-13.**

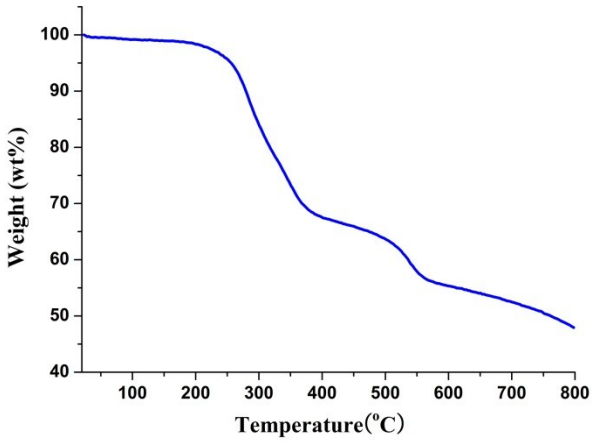

Figure S14. TGA curve of **VMOP-14.**

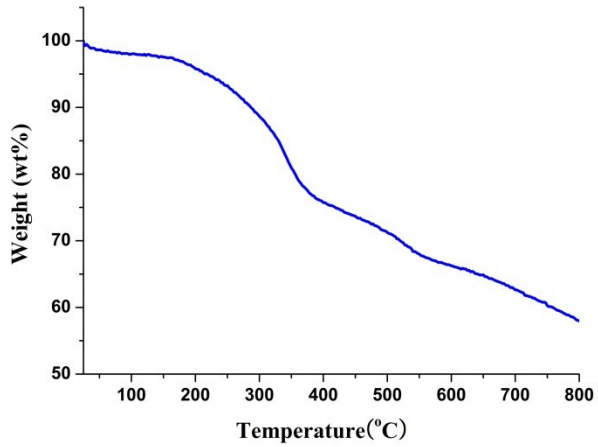

Figure S15. TGA curve of **VMOP-15.**

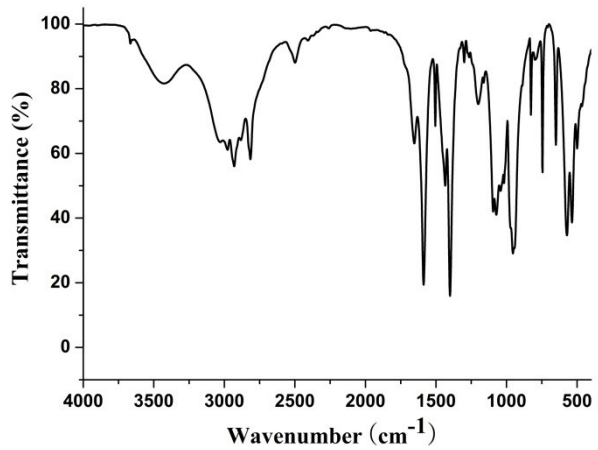

Figure S16. IR spectrum of **VMOP-11.**

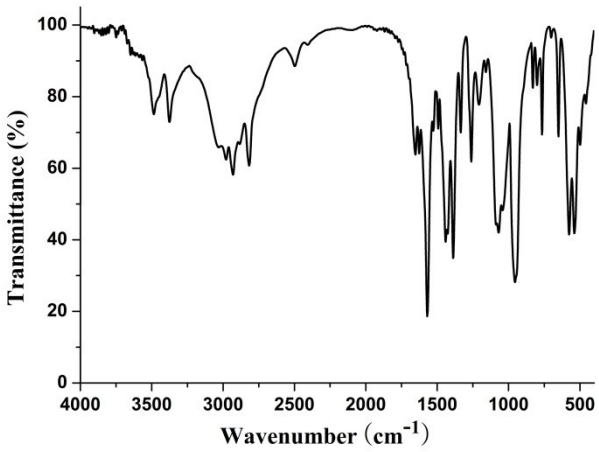

Figure S17. IR spectrum of **VMOP-12.**

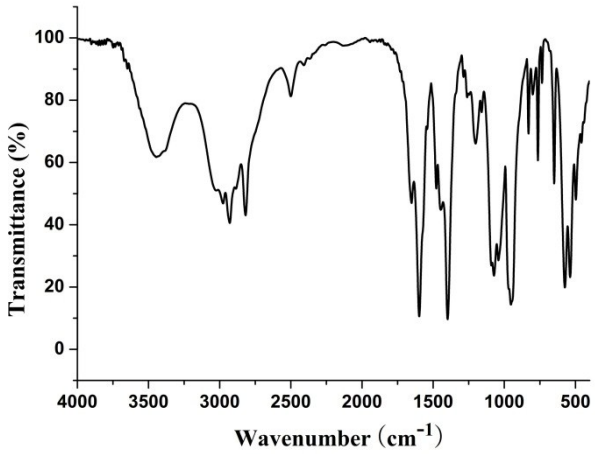

Figure S18. IR spectrum of **VMOP-13**.

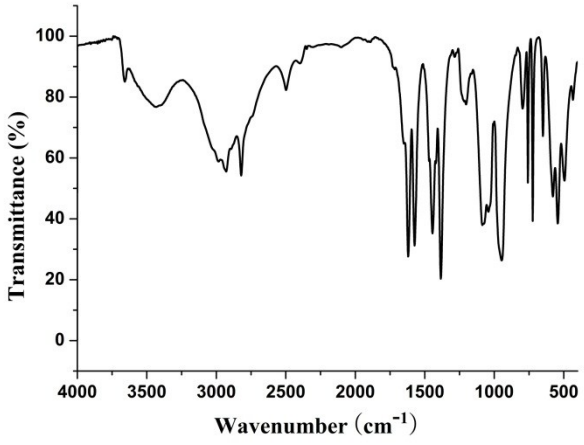

Figure S19. IR spectrum of **VMOP-14.**

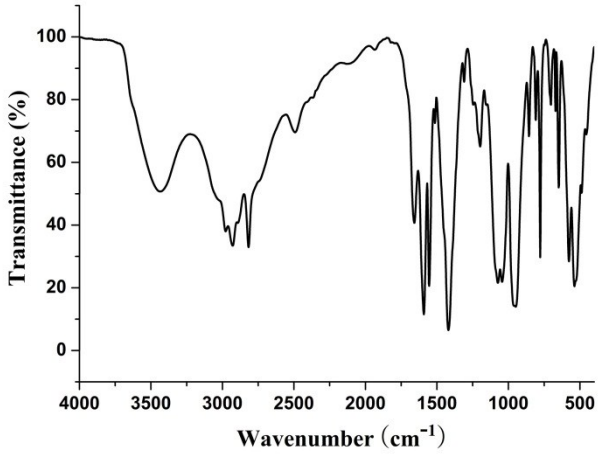

Figure S20. IR spectrum of **VMOP-15.**

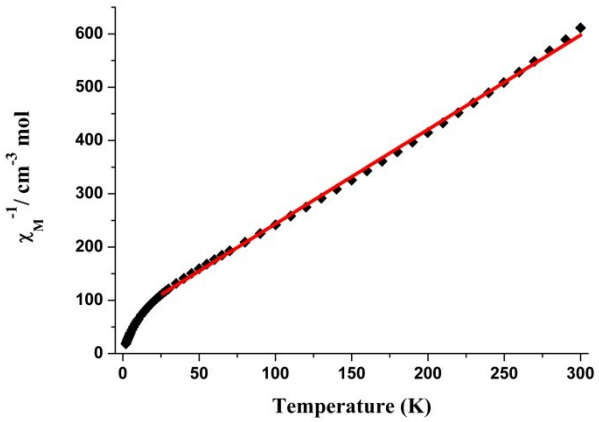

Figure S21. The temperature dependence of the inverse magnetic susceptibility χ_M^{-1} for **VMOP-14** between 2 and 300 K. The solid red line was generated from the best fit by the Curie-Weiss expression in the range of 25–300 K with the Curie constant C = 0.56 cm^3 K mol^{-1} and the Weiss constant θ = –37.38 K.

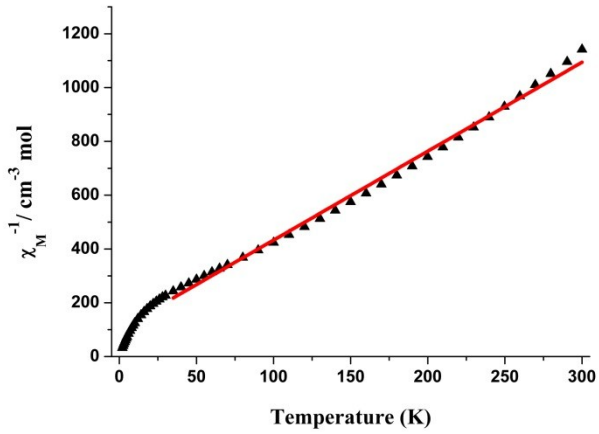

Figure S22. The temperature dependence of the inverse magnetic susceptibility χ_M^{-1} for **VMOP-15** between 2 and 300 K. The solid red line was generated from the best fit by the Curie-Weiss expression in the range of 35–300 K with the Curie constant C = 0.30 cm^3 K mol^{-1} and the Weiss constant θ = –30.97 K.

References

1 K. Barthelet, J. Marrot, G. Férey and D. Riou, *Chem. Commun*., 2004, 520−521.
2 K. Barthelet, J. Marrot, D. Riou and G. Férey, *Angew. Chem. Int. Ed*., 2002, **114**, 291–294.
3 K. Barthelet, D. Riou and G. Férey, *Chem. Commun*., 2002, 1492–1493.
4 K. Barthelet, D. Riou, M. Nogues and G. Férey, *Inorg. Chem*., 2003, **42**, 1739−1743.
5 Y. Liu, S. Couck, M. Vandichel, M. Grzywa, K. Leus, S. Biswas, D. Volkmer, J. Gascon, F. Kapteijn, J. F. M. Denayer, M. Waroquier, V. Van Speybroeck and P. Van Der Voort, *Inorg. Chem.,* 2013, **52**, 113−120.
6 S. Biswas, S. Couck, M. Grzywa, J. F. M. Denayer, D. Volkmer and P. Van Der Voort, *Eur. J. Inorg. Chem.,* 2012, 2481–2486.
7 Z. J. Zhang, L. Wojtas and M. J. Zaworotko, *Chem. Sci*., 2014, **5**, 927−931.
8 Z. X. Zhang, W. Y. Gao, L. Wojtas, Z. J. Zhang and M. J. Zaworotko, *Chem. Commun.*, 2015, **51**, 9223−9226.
9 Y. T. Zhang, X. L. Wang, E. L. Zhou, X. S. Wu, B. Q. Song, K. Z. Shao and Z. M. Su, *Dalton Trans*., 2016, **45**, 3698–3701.
10 (a) K. Leus, S. Couck, M. Vandichel, G. Vanhaelewyn, Y. Y. Liu, G. B. Marin, I. Van Driessche, D. Depla, M. Waroquier, V. Van Speybroeck, J. F. M. Denayerb and P. Van Der Voort, *Phys. Chem. Chem. Phys*., 2012, 14, 15562–15570; (b) J. Q. Shen, Y. Zhang, Z. M. Zhang, Y. G. Li, Y. Q. Gao and E. B. Wang, *Chem. Commun*., 2014, 50, 6017–6019.